

Synthesis and Characterization of an Isorecticular Family of Calixarene-Capped Porous Coordination Cages

Michael R. Dworzak, Meaghan M. Deegan, Glenn P. A. Yap, and Eric D. Bloch*

Cite This: *Inorg. Chem.* 2021, 60, 5607–5616

Read Online

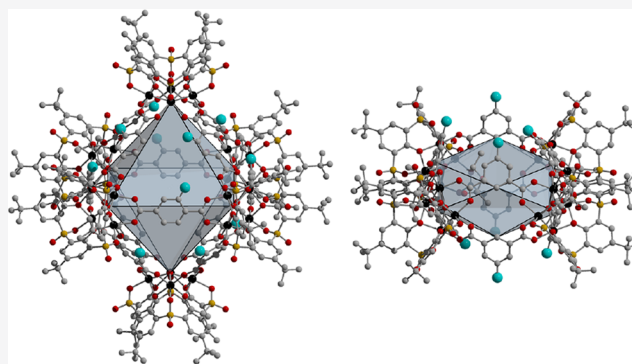
ACCESS |

Metrics & More

Article Recommendations

Supporting Information

ABSTRACT: Functionalization of permanently porous coordination cages has been used to tune phase, surface area, stability, and solubility in this promising class of adsorbents. For many cages, however, these properties are intricately tied together, and installation of functional groups, for example, to increase solubility often leads to a decrease in surface area. Calixarene-capped cages offer the advantage in that they are cluster-terminated cages whose solid-state packing, and thus surface area, is typically governed by the nature of the capping ligand rather than the bridging ligand. In this work we investigate the influence of ligand functionalization on two series of isorecticular Ni(II)- and Co(II)-based calixarene-capped cages. The two types of materials described are represented as octahedral and rectangular prismatic coordination cages and can be synthesized in a modular manner, allowing for the substitution of dicarboxylate bridging ligands and the introduction of functional groups in specific locations on the cage. We ultimately show that highly soluble cages can be obtained while still having access to high surface areas for many of the isolated phases.



INTRODUCTION

Permanently porous coordination cages have received renewed interest over the past few years as a result of their status as high surface area molecular materials. In this regard, they have been studied for gas separation,^{1,2} gas storage,^{3,4} catalysis,^{5,6} host–guest chemistry,⁷ and a number of additional applications. As a result of their molecular nature, they offer significant benefits as compared to typical three-dimensional porous solids, including metal–organic frameworks, with their potential solubility making them well suited for solution-phase assembly routes.^{8,9} In addition to this, their modularity allows for the straightforward incorporation of functional groups^{10–15} and provides a level of compatibility toward postsynthetic modification strategies that is not possible for extended structures.^{16–18} Functionalization of permanently porous coordination cages has been used as a means to tune solubility,¹⁹ gas adsorption properties,²⁰ and bulk density²¹ and has been targeted at bridging ligands,²² capping ligands,²³ and coordinatively unsaturated transition metal cation sites.²⁴

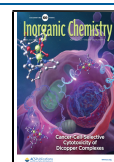
For some porous coordination cages, however, ligand functionalization can interfere with materials synthesis and result in the formation of extended solids or nonporous molecular materials. This is particularly the case for paddlewheel-based cuboctahedral or octahedral structures with isophthalic acid or carbazoledicarboxylic acid, respectively. Both 5-position functionalization of isophthalic acid and 9-position functionalization of carbazoledicarboxylate have been widely reported, and the nature of the functional group

can determine whether molecular materials, two-dimensional MOFs, or three-dimensional MOFs are isolated.^{22,25} In addition to this, functional groups have a pronounced effect on thermal stability, solubility, crystal packing, and porosity.²⁶ We have found that for most paddlewheel-based cages solubility and porosity are inexorably linked where the highest surface area cages are insoluble and the most soluble cages display limited porosity.²¹

In addition to ligand-terminated paddlewheel-based cages (Figure 1), functional groups can similarly be tuned in cluster-terminated cages, either on the bridging ligand or on the cluster caps. Ligand functionalization, for example, has been used to control the nuclearity and solid-state packing in zirconocene-based cages where the ratio between length and width of the terephthalate-based bridging ligand has great influence over the shape of the product cage(s).²⁷ A subset of cluster-capped permanently porous coordination cages are also amenable to functionalization routes where either the bridging or capping ligand can be modified to tune material properties.^{28,29} The CIAC (Changchun Institute of Applied

Received: December 4, 2020

Published: March 30, 2021



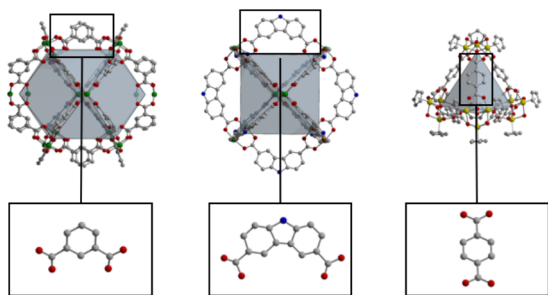


Figure 1. Cuboctahedral (left) and octahedral (center) paddlewheel-based cages represent ligand-terminated structures and are amenable to a wide range of surface functionalization. Cyclopentadienyl-capped zirconium cages (right) can be functionalized on the linear ligands that typically comprise these structures.

Chemistry) and MOSC (metal–organic supercontainer) families of porous cages are relevant examples in this regard and use calixarenes, a tunable class of cyclic oligomers, to form capped metal clusters as nodes in cage formation.^{23,30–34} Calixarene-type molecules have been isolated with up to 90 phenol units in their structures³⁵ and are commonly encountered as 4-unit oligomers as caps in porous cages. These four phenol units can then be bridged by either CH_2 , S, or SO_2 units, resulting in calix[4]arenes (C4A),³⁶ thiacalix[4]arenes (TC4A),³⁷ or sulfonylcalix[4]arenes (SC4A),^{38,39} respectively. These most often contain *tert*-butyl groups on their upper rim with the phenol hydroxyl groups on the lower rim. Among these three types of calixarenes, SC4As (Figure 2)

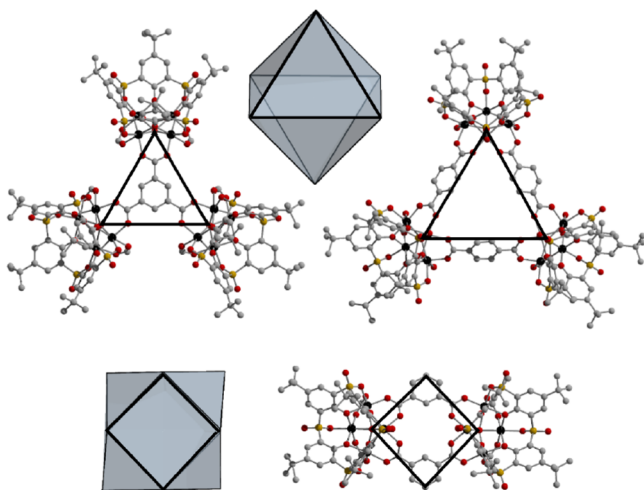


Figure 2. Calixarene-based cages typically adopt octahedral structures where bridging ligands lie at either the face (top left) or edge (top right) of the octahedron. Isophthalate-based cages are related structures and adopt a truncated octahedral geometry.

offer milder synthesis conditions due to the oxygen atoms of the $-\text{SO}_2$ groups. The use of oxygen as a coordination site allows for the formation of a more ideal octahedral geometry between the metal cation and coordination atoms as opposed to a more strained geometry seen when using TC4A.⁴⁰ As such, they are compatible with tetranuclear clusters that have been isolated for Mg, Fe, Co, Ni, and Zn with a variety of di- and tricarboxylate ligands.⁴¹ The tetranuclear clusters in these cages contain a μ_4 atom at their center which has been reported in the past as a variety of species including O, OH^- ,

H_2O ,⁴³ or Cl^- .⁴⁴ The μ_4 species can also impart charge on what would otherwise be a neutral cage, which can have important implications for their stability, surface area, and solubility.⁴⁰

When TC4A and SC4A are used as SBUs, the rigidity of the capping node allows for reliable structural regularity based on the binding site angle of the bridging ligand. Specifically, when a tritopic bridging ligand is used (i.e., trimesic acid), octahedral molecular cages form with six SC4A metal cluster caps and eight bridging ligands sitting in the faces of the octahedral structure. When ditopic ligands (i.e., terephthalic acid, isophthalic acid, etc.) are used, the resulting cage shape can vary. For example, linear ligands still allow for octahedral geometry but with 12 linear bridging ligands on the edges of the structure, but when ligands of other angles become introduced, the resulting geometry becomes more complex in an effort to orient cap/cluster and ligand in the least strained orientation (Figure 3).

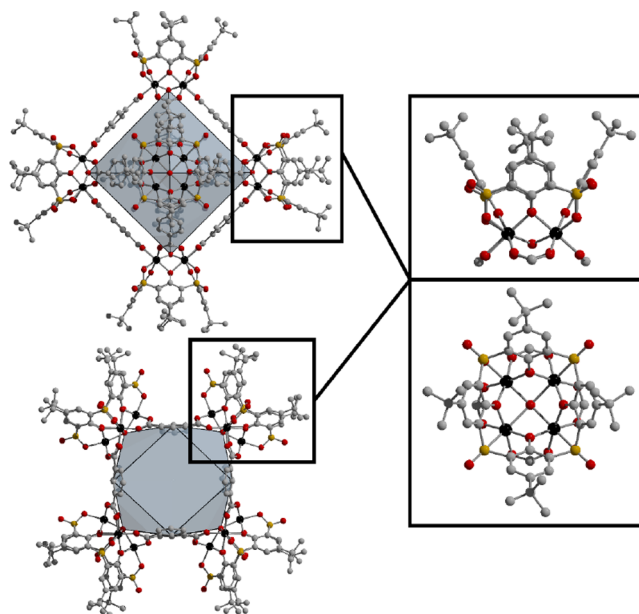


Figure 3. Structures of octahedral calixarene-capped cages based on terephthalate (top) and isophthalate (bottom). In these structures, the 2- and 5-position of the ligand groups, respectively, are potentially functionalizable. These structures have previously been termed type II or type III MOSCs.

Four subclasses of sulfonylcalix[4]arene-capped cages have been previously reported that were based on tritopic, linear ditopic, 120° bent ditopic, and 109.5° bent ditopic ligands with a variety of transition metals.^{29,45,46} Functionalization of these cages includes altering the metal in the tetranuclear cluster, adding or removing alkyl groups from the upper rim of the SC4A cap, and adding functional groups to the bridging ligand at a given position.^{29,45} The synthesis of these functionalized isorecticular cages has been limited to a nickel cage made with 5-sulfoisophthalic acid monolithium salt ($\text{Ni}(\text{S}-\text{SO}_3)$) and two terephthalate-based nickel structures containing 2-amino-terephthalic acid ($\text{Ni}(\text{2-NH}_2)$) and the other with 2-bromoterephthalic acid ($\text{Ni}(\text{2-Br})$).^{44,45}

It is important to note that, in contrast to paddlewheel- or zirconium-based cages, the solid-state packing of these types of cages has been largely governed by the nature of the functional

groups on the calixarene caps rather than ligands on the carboxylate ligands that comprise the structures. This offers a unique opportunity to potentially tune the solubility and thus processability of these cages without altering the structures of the materials in the solid state. Here, we present the design, synthesis, and characterization of eight novel calixarene-capped porous cages, six of which have been characterized by single-crystal X-ray diffraction.

EXPERIMENTAL SECTION

General Considerations. All handling of materials and syntheses were performed in air unless otherwise specified. All solvents, metal salts, and organic ligands were obtained from commercial sources and used without further purification. Me-H₂-bdc,⁴⁷ OProp-H₂bdc,²² and OHept-H₂bdc⁴⁸ were prepared via previously reported synthetic protocols.

Physical Methods. Thermogravimetric analyses (TGA) were performed with a TA Q5000 SA under an N₂ flow. Samples were loaded onto a tared aluminum pan and heated from room temperature to 600 °C at a rate of 2 °C/min. Powder X-ray diffraction patterns were collected by using a Bruker D8 X-ray diffractometer with a LynxEye position-sensitive detector operating with a Cu K α_1 X-ray generator ($\lambda = 1.54 \text{ \AA}$). ¹H and ¹³C NMR spectra were measured by using a Bruker 400 MHz spectrometer, with data processed by using MestReNova NMR software. Infrared (IR) spectra were collected by using a Bruker ALPHA II ATR-IR spectrometer with OPUS data processing software.

Gas Adsorption Measurements. Synthesized materials were solvent exchanged with EtOH over the course of 3 days, replacing the solvent once per day. Materials were obtained as free-flowing powders by decanting the solvent and then evacuating the samples for 30 min under dynamic vacuum at room temperature. Samples for gas adsorption were activated under a positive nitrogen flow, with the optimal activation temperature for each material determined by increasing the activation temperature by 25 °C and recording single-point N₂/CO₂ uptakes. Low-pressure gas adsorption measurements up to 1.1 bar were recorded on a Micromeritics 3Flex gas adsorption analyzer. N₂ and CO₂ surface areas were measured at 77 and 195 K, respectively. Prior to measurements, samples were considered activated when their outgas rate under static vacuum was $\leq 2 \mu\text{bar}/\text{min}$. All measurements were performed with ultrahigh-purity gases. High-pressure isotherms were collected on a Sievert apparatus (PCT-Pro-2000 from Hy-Energy Scientific Instruments) using ultrahigh-purity gases. The total adsorption was calculated by using NIST thermochemical properties of CH₄ and the pore volume of each material, as determined via 77 K N₂ adsorption experiments.

Synthesis of *p*-tert-Butylsulfonfylcalix[4]arene (TC4A). To a 1 L round-bottom flask, *p*-tert-butylphenol (64.5 g, 0.43 mol), elemental sulfur (27.5 g, 0.86 mol), NaOH (8.86 g, 0.215 mol), and tetraethylene glycol dimethyl ether (19 mL) were added and stirred under a flow of nitrogen. The mixture was heated to 230 °C over 4 h and held at this temperature overnight. The mixture was allowed to cool to room temperature, yielding a dark-brown solid to which toluene (35 mL) and 4 M H₂SO₄ (78 mL) were added. The flask was then sonicated for 30 min, and the solubilized material was transferred to a separatory funnel. The organic phase was collected, and MeOH (400 mL) was added, precipitating the product as a light-brown powder that could be isolated by vacuum filtration. This process was repeated until all of the initially generated solid was dissolved. The collected product was dried at 120 °C for 24 h prior to use.

Synthesis of *p*-tert-Butylsulfonfylcalix[4]arene (SC4A). In a 1 L round-bottom flask, TC4A (7 g, 46.7 mmol) and sodium perborate tetrahydrate (14 g, 91.0 mmol) were added to a mixture of chloroform (210 mL) and acetic acid (350 mL). The resultant solution was heated with stirring at 50 °C for 18 h. After the solution cooled to room temperature, H₂O (300 mL) was added, and the solution was transferred to a separatory funnel. The organic layer was collected, and the solvent was removed via rotary evaporation before an excess of Et₂O was added; the precipitated white solid was

collected via vacuum filtration. The product was dried at 120 °C for 24 h prior to use.

Synthesis of [(Ni₄OHsc4A)₆(Btc)₈]⁶⁻ (Ni-Btc).²⁹ To a 20 mL scintillation vial, Ni(NO₃)₂·6H₂O (145 mg, 0.5 mmol), 1,3,5-benzenetricarboxylic acid (69.3 mg, 0.33 mmol), and SC4A (85 mg, 0.1 mmol) were added and solvated in DMF (10 mL). The vial was heated to 100 °C in a dry bath for 24 h before cooling slowly to room temperature. Partial precipitation of the product as a green crystalline solid was observed upon cooling, with additional crystal growth observed after standing for an additional 24 h at room temperature. The material was activated for gas adsorption measurements at 110 °C.

Synthesis of [(Co₄OHsc4A)₆(Btc)₈]⁶⁻ (Co-Btc).²⁹ To a 20 mL scintillation vial, CoCl₂·6H₂O (119 mg, 0.5 mmol), 1,3,5-benzenetricarboxylic acid (69.3 mg, 0.33 mmol), and SC4A (85 mg, 0.1 mmol) were added and solvated in DMF (10 mL). The vial was heated to 100 °C in a dry bath for 24 h before cooling slowly to room temperature. Partial precipitation of the product as a green crystalline solid was observed upon cooling, with additional crystal growth observed after standing for an additional 24 h at room temperature. The material was activated for gas adsorption measurements at 110 °C.

Synthesis of [(Ni₄OHsc4A)₆(Bdc)₁₂]⁶⁻ (Ni-*p*-Bdc).⁴⁵ To six 20 mL scintillation vials, Ni(NO₃)₂·6H₂O (145 mg, 0.5 mmol), 1,4-benzenedicarboxylic acid (54.8 mg, 0.33 mmol), and SC4A (85 mg, 0.1 mmol) were added and solvated in DMF (10 mL). The vials were heated to 100 °C in a dry bath for 24 h before cooling slowly to room temperature. Vapor diffusion of Et₂O into the resultant mixtures yielded the product as a green polycrystalline solid. X-ray quality single crystals were obtained upon vapor diffusion with EtOAc rather than Et₂O. The material was activated for gas adsorption measurements at 300 °C.

Synthesis of [(Co₄OHsc4A)₆(Bdc)₁₂]⁶⁻ (Co-*p*-Bdc).⁴⁵ To six 20 mL scintillation vials, Co(NO₃)₂·6H₂O (145 mg, 0.5 mmol), 1,4-benzenedicarboxylic acid (54.8 mg, 0.33 mmol), and SC4A (85 mg, 0.1 mmol) were added and solvated in DMF (10 mL). The vials were heated to 100 °C in a dry bath for 24 h before cooling slowly to room temperature. Vapor diffusion of Et₂O into the resultant mixtures yielded the product as a red polycrystalline solid. X-ray quality single crystals were obtained upon vapor diffusion with EtOAc rather than Et₂O. The material was activated for gas adsorption measurements at 275 °C.

Synthesis of [(Ni₄OHsc4A)₄(Bdc)₈]⁴⁻ (Ni-*m*-Bdc).⁴⁶ To six 20 mL scintillation vials, Co(NO₃)₂·6H₂O (145 mg, 0.5 mmol), 1,3-benzenedicarboxylic acid (54.8 mg, 0.33 mmol), and SC4A (85 mg, 0.1 mmol) were added and solvated in DMF (10 mL). The vials were heated to 100 °C in a dry bath for 24 h before cooling slowly to room temperature. Vapor diffusion of Et₂O into the resultant mixtures yielded the product as a green polycrystalline solid. X-ray quality single crystals were obtained upon vapor diffusion with EtOAc rather than Et₂O. The material was activated for gas adsorption measurements at 250 °C.

Synthesis of [(Co₄OHsc4A)₄(Bdc)₈]⁴⁻ (Co-*m*-Bdc).⁴⁶ To six 20 mL scintillation vials, Co(NO₃)₂·6H₂O (145 mg, 0.5 mmol), 1,3-benzenedicarboxylic acid (54.8 mg, 0.33 mmol), and SC4A (85 mg, 0.1 mmol) were added and solvated in DMF (10 mL). The vials were heated to 100 °C in a dry bath for 24 h before cooling slowly to room temperature. Vapor diffusion of EtOAc into the resultant mixtures yielded the product as a red crystalline solid. The material was activated for gas adsorption measurements at 150 °C.

Synthesis of [(Ni₄OHsc4A)₄(SO₃⁻Li⁺-Bdc)₈]⁴⁻ (Ni-(5-Sulfo)).⁴⁶ To a 20 mL scintillation vial, Ni(NO₃)₂·6H₂O (145 mg, 0.5 mmol), 5-sulfo-1,3-benzenedicarboxylic acid monolithium salt (55.5 mg, 0.22 mmol), and SC4A (85 mg, 0.1 mmol) were added and solvated in DMF (10 mL). The vials were heated to 100 °C in a dry bath for 24 h before cooling slowly to room temperature. Partial precipitation of the product as a green crystalline solid was observed upon cooling, with additional crystal growth observed after standing for an additional 24 h at room temperature. The material was activated for gas adsorption measurements at 325 °C.

Synthesis of [(Co₄OHsc4A)₄(SO₃⁻Li⁺-Bdc)₈]⁴⁻ (Co-(5-Sulfo)). To a 20 mL scintillation vial, Co(NO₃)₂·6H₂O (145 mg, 0.5 mmol), 5-sulfo-1,3-benzenedicarboxylic acid monolithium salt (55.5 mg, 0.22 mmol), and SC4A (85 mg, 0.1 mmol) were added and solvated in DMF (10 mL). The vials were heated to 100 °C in a dry bath for 24 h before cooling slowly to room temperature. Partial precipitation of the product as a pink crystalline solid was observed upon cooling, with additional crystal growth observed after standing for an additional 24 h at room temperature. The material was activated for gas adsorption measurements at 325 °C.

Synthesis of [(Ni₄OHsc4A)₆(methyl-Bdc)₁₂]⁶⁻ (Ni-(2-Methyl)). To six 20 mL scintillation vials, Ni(NO₃)₂·6H₂O (145 mg, 0.5 mmol), 2-methyl-1,4-benzenedicarboxylic acid (59.5 mg, 0.33 mmol), and SC4A (85 mg, 0.1 mmol) were added and solvated in DMF (10 mL). The vials were heated to 100 °C in a dry bath for 24 h before cooling slowly to room temperature. Vapor diffusion of EtOAc into the resultant mixtures yielded the product as a green crystalline solid. The material was activated for gas adsorption measurements at 250 °C.

Synthesis of [(Ni₄OHsc4A)₄(methyl-Bdc)₈]⁴⁻ (Ni-(5-Methyl)). To six 20 mL scintillation vials, Ni(NO₃)₂·6H₂O (145 mg, 0.5 mmol), 5-methyl-1,3-benzenedicarboxylic acid (59.5 mg, 0.33 mmol), and SC4A (85 mg, 0.1 mmol) were added and solvated in DMF (10 mL). The vials were heated to 100 °C in a dry bath for 24 h before cooling slowly to room temperature. Vapor diffusion of Et₂O into the resultant mixtures yielded the product as a green polycrystalline solid. X-ray quality single crystals were obtained upon vapor diffusion with EtOAc rather than Et₂O. The material was activated for gas adsorption measurements at 225 °C.

Synthesis of [(Ni₄OHsc4A)₆(Br-Bdc)₁₂]⁶⁻ (Ni-(2-Br)). To six 20 mL scintillation vials, Ni(NO₃)₂·6H₂O (119 mg, 0.5 mmol), 2-bromo-1,4-benzenedicarboxylic acid (80.9 mg, 0.33 mmol), and SC4A (85 mg, 0.1 mmol) were added and solvated in DMF (10 mL). The vials were heated to 100 °C in a dry bath for 24 h before cooling slowly to room temperature. Vapor diffusion of Et₂O into the resultant mixtures yielded the product as a green polycrystalline solid. X-ray quality single crystals were obtained upon vapor diffusion with EtOAc rather than Et₂O. The material was activated for gas adsorption measurements at 150 °C.

Synthesis of [(Ni₄OHsc4A)₄(Br-Bdc)₈]⁴⁻ (Ni-(5-Br)). To six 20 mL scintillation vials, Ni(NO₃)₂·6H₂O (119 mg, 0.5 mmol), 5-bromo-1,3-benzenedicarboxylic acid (80.9 mg, 0.33 mmol), and SC4A (85 mg, 0.1 mmol) were added and solvated in DMF (10 mL). The vials were heated to 100 °C in a dry bath for 24 h before cooling slowly to room temperature. Vapor diffusion of EtOAc into the resultant mixtures yielded the product as a green crystalline solid. The material was activated for gas adsorption measurements at 225 °C.

Synthesis of [(Ni₄OHsc4A)₆(Dobdc)₁₂]⁶⁻ (Ni-(Dobdc)). To six 20 mL scintillation vials, NiCl₂·6H₂O (119 mg, 0.5 mmol), 2,5-dihydroxy-1,4-benzenedicarboxylic acid (65.4 mg, 0.33 mmol), and SC4A (85 mg, 0.1 mmol) were added and solvated in DMF (10 mL). The vials were heated to 100 °C in a dry bath for 24 h before cooling slowly to room temperature. Vapor diffusion of CHCl₃ into the resultant mixtures yielded the product as a green crystalline solid. The material was activated for gas adsorption measurements at 250 °C.

Synthesis of [(Ni₄OHsc4A)₄(OProp-Bdc)₈]⁴⁻ (Ni-(5-OProp)). To six 20 mL scintillation vials Ni(NO₃)₂·6H₂O (145 mg, 0.5 mmol), 5-propoxy-1,3-benzenedicarboxylic acid (74.0 mg, 0.33 mmol), and SC4A (85 mg, 0.1 mmol) were added and solvated in DMF (10 mL). The vials were heated to 100 °C in a dry bath for 24 h before cooling slowly to room temperature. Vapor diffusion of MeOH into the resultant mixtures yielded the product as a green crystalline solid. The material was activated for gas adsorption measurements at 275 °C.

Synthesis of [(Co₄OHsc4A)₄(OHept-Bdc)₈]⁴⁻ (Co-(5-OHept)). To six 20 mL scintillation vials Co(NO₃)₂·6H₂O (145 mg, 0.5 mmol), 5-heptoxyisophthalic acid (92.4 mg, 0.33 mmol), and SC4A (85 mg, 0.1 mmol) were added and solvated in DMF (10 mL). The vials were heated to 100 °C in a dry bath for 24 h before cooling slowly to room temperature. Vapor diffusion of MeOH into the resultant mixtures yielded the product as a pink crystalline solid. The material was activated for gas adsorption measurements at 225 °C.

Monolith Formation. To three glass cells with internal diameters of 5 mm and an internal height of 66 mm, 6, 12.5, and 25 mg of Ni-(2-Me) were dosed. Each sample was solvated in 1 mL of benzene and frozen in liquid nitrogen. Quartz wool was then introduced at the top of each glass cell on top of each frozen sample before being transferred to gas adsorption measurement tubes, submerged in liquid nitrogen. The samples were subjected to reduced pressure, and once the vacuum pressure reached below 0.01 mbar, the liquid nitrogen bath was removed and replaced with an ice bath which remained for 18 h or until the vacuum pressure returned to <0.01 mbar.

Single-Crystal X-ray Diffraction. X-ray structural analysis was performed for Ni-(2-Methyl), Ni-(5-Methyl), Ni-(dobdc), Ni-(2-Br), Ni-(5-OProp), and Co-(5-OHept). Crystal data and refinement details are shown in Table 1. Crystals were mounted by using viscous

Table 1. Cage Solubility

cage	a	b	c	d	e	f	g	h
Ni-(btc)	s	s	s	i	i	i	i	i
Co-(btc)	s	s	s	i	i	i	i	i
Ni-(p-bdc)	s	s	s	p	i	i	i	i
Co-(p-bdc)	s	s	s	i	s	i	i	i
Ni-(m-bdc)	s	s	s	s	s	s	i	i
Co-(m-bdc)	s	s	s	s	s	i	i	i
Ni-(5-Sulfo)	s	i	i	i	i	i	i	i
Co-(5-Sulfo)	s	i	i	i	i	i	i	i
Ni-(2-Me)	s	s	s	p	i	s	p	i
Ni-(5-Me)	s	s	s	s	s	s	s	s
Ni-(2-Br)	s	s	s	s	s	i	i	i
Ni-(5-Br)	s	s	i	i	p	i	i	i
Ni-(dobdc)	s	s	p	p	s	s	s	i
Ni-(5-OPr)	s	s	s	s	s	s	i	i
Co-(5-OHept)	s	s	s	s	s	s	s	p

^aDMF. ^bChloroform. ^cMethylene chloride. ^dAcetone. ^eTHF. ^fBenzene. ^gToluene. ^hEthyl acetate.

oil onto a plastic mesh and cooled to the data collection temperature. Data were collected on a Bruker-AXS APEX II DUO CCD diffractometer with Cu K α radiation ($\lambda = 1.54178 \text{ \AA}$) focused with Goebel mirrors. Unit cell parameters were obtained from 48 data frames, 0.5° ω , from different sections of the Ewald sphere. The unit-cell dimensions, equivalent reflections, and systematic absences in the diffraction data are uniquely consistent with R-3 and R3 for Ni-(2-Methyl), Ni-(dobdc), and Ni-(2-Br) and with C2/c and Cc for Ni-(5-OProp). No symmetry higher than triclinic was observed for Ni-(5-Methyl) and Co-(5-OHept). Refinement in the centrosymmetric space group options, R-3, C2/c, and P-1, yielded chemically reasonable and computationally stable results of refinement. The data were treated with multiscan absorption corrections.⁴⁹ Structures were solved by using intrinsic phasing methods⁵⁰ and refined with full-matrix, least-squares procedures on F².

Residual electron density, solvent molecules, and atoms that cannot be assigned a reasonable model were treated as diffused electron density by using the Olex2⁵¹ implementation of Squeeze. In Co-(5-OHept), the ligand alkyl chain was confirmed by digestion followed by NMR spectroscopy, and thus the electron density that was deducted from the diffused alkyl chain ends could be assigned. A dimethylammonium ion was located H-bonded to two DMF solvent molecules in Co-(5-OHept); thus, accessible voids that were too small to fit DMF were assigned to contain dimethylammonium. Although the assignments of void contents were based on the best spatial and electron count fit of the predominant reaction solvents, we cannot discount the possibility of alternative void contents that might consist of a combination of water, minor solvents, thermal decomposition products of amide solvents, or solvated metal ions. In initial solutions of Ni-(dobdc) there appeared to be a heavy atom containing group that was severely disordered and subsequently removed from the model; hence, its formula weight could be

underestimated. The structures are located on special positions: on 3-fold axes for Ni-(2-Methyl) and Ni-(2-Br); on 6-fold improper axis for Ni-(dobdc); on a 2-fold for Ni-(5-OProp); and on inversion for Ni-(5-Methyl) and Co-(5-OHept).

The symmetry unique 2,5-dihydroxyl phthalate ligands in Ni-(dobdc) were found disordered in two positions with independently refined site occupancy ratios of 52/48 and 52/48. The bromophthalate ligands in Ni-(2-Br) were found to be each disordered, in multiple positions, were treated as rigid groups based on an ordered bromophthalate ligand in a previously reported structure,⁵² and were each restrained to have unitary occupancy per ligand.

These compounds consistently deposit as multiple, high mosaicity, weakly diffracting crystals, and the results herein represent the best of several trials. To compensate for the low-resolution data, various constraints and restraints were applied. To further conserve a reasonable data/parameter ratio, all atoms in Co-(5-OHept) and the solvated cation complexes in Ni-(2-Methyl) and Ni-(5-OProp) were refined with isotropic displacement parameters. All other non-hydrogen atoms were refined with anisotropic displacement parameters. H atoms in cocrystallized methanol and water molecules and those on the hydroxyl groups in Ni-(dobdc) could be neither located nor calculated and were ignored. All other H atoms were treated as idealized contributions with geometrically calculated positions and with U_{iso} equal to $(1.2-1.5)U_{eq}$ of the attached carbon atom. Atomic scattering factors are contained in the SHELXTL program library. The structures have been deposited at the Cambridge Structural Database under the following CCDC deposition numbers: 2016862–2016867.

RESULTS AND DISCUSSION

The syntheses of calixarene-based coordination cages typically rely on the use of high-temperature solvothermal or hydrothermal conditions where a one-pot reaction of metal salt, bridging ligand, and calixarene cap affords the targeted cage. It has generally been shown that relatively more forcing conditions are required to afford thiacalixarene-based cages, likely a result of the strained geometry at the metal cation sites that comprise the materials. By comparison, sulfonylcalix[4]-arene capped cages are isolable under more facile conditions. In this work, synthesis of three novel octahedral and five novel truncated octahedral structures was achieved via the reaction of 5-sulfoisophthalic acid monolithium salt (5-Sulfo bdc), 2-methylterephthalic acid (2-Methyl bdc), 5-methylisophthalic acid (5-Methyl bdc), 2-bromoterephthalic acid (2-Bromo bdc), 5-bromoisophthalic acid (5-Bromo bdc), 2,5-dihydroxyterephthalic acid (dobdc), 5-propylisophthalic acid (5-Propoxy bdc), and 5-heptoxylisophthalic acid (5-Heptoxy bdc) with the appropriate metal salts under solvothermal conditions affording Co-(5-Sulfo), Ni-(2-Methyl), Ni-(5-Methyl), Ni-(2-Br), Ni-(5-Br), Ni-(dobdc), Ni-(5-Propoxy), and Co-(5-Heptoxy), respectively. All of the materials based on functionalized isophthalic acid ligands afford truncated octahedral structures while the terephthalate-based cages adopt octahedral structures.

For the preparation of functionalized cages, we screened the reaction of the aforementioned ligands with hydrated cobalt(II) and nickel(II) nitrate and chloride salts in the presence of capping ligand. Ultimately, the cages we report here are readily obtained by reacting the appropriate metal salts and their corresponding ligand in the presence of SC4A at 100 °C in DMF for 24 h. Although moderate color changes were observed over the course of reactions, and in contrast to the synthesis of most MOFs and many coordination cages, no solid product phase was observed throughout the solvothermal reactions. However, M-(5-sulfo) (M = Co, Ni) crystals formed

upon cooling of the reaction mixtures. To obtain crystalline material for the balance of the ligands investigated here, vapor diffusion of an antisolvent into the reaction mixture was required. Large green and red crystals of nickel- and cobalt-based MOSCs, respectively, form upon diffusion of Et₂O into solutions in 20 mL scintillation vials over the course of 3–5 days. These reactions typically produced large amounts of highly crystalline solids with overall yields ranging from 20% to 70% based on the calixarene cap. Diffraction-quality single crystals were obtained via diffusion of EtOAc into DMF solutions in 4 mL scintillation vials over the course of ~1 week. Notably, for the truncated octahedral (isophthalic acid-based) cages, increasingly polar antisolvents were required as the bulk and/or chain length of appended functional groups were increased.

X-ray diffraction data collected for these materials confirmed their isostructural nature and further showed that solid-state packing of these structures was generally not perturbed by ligand functionalization. For both terephthalate- and isophthalate-based cages, each molecule generally crystallized in the same space group as the unfunctionalized parent structures, with control over solid-state packing dominated by the interactions between the calixarene caps rather than interactions between the incorporated bridging ligand functionality. The previously reported nickel-terephthalic acid cage and all novel 1,4-bdc derivatives reported here crystallize in the rhombohedral space group *R*-3. For these octahedral cages, the incorporated functional groups sit in the pore windows of the cage with no apparent intercalation interactions between the ligand-appended groups, and all structures show minimal deviations in their unit cell parameters (all axes ± 1.5 Å). A similar trend is observed for the isophthalate-based cages, most of which crystallize in the triclinic space group *P*-1. For these materials, the structures were packed with all of calixarene ligands oriented toward one another in the same plane and incorporated functional groups protruding toward the space between sheets of cages. This perturbs the separation between sheets of cages and slightly alters the way cages pack in each sheet. This results in some expansion of the unit cell parameters for the truncated octahedra upon incorporation of functional groups. For one of the synthesized materials, Ni-(5-Methyl), the incorporation of a functional group resulted in the crystallization of this material in the monoclinic space group *C*2/*c*. This was not generally observed upon incorporation of larger functional groups, as the packing for the Co-(5-Heptoxy) structure was analogous to other isophthalate-based calixarene cages. In this case, two-dimensional layers of cages are more widely spaced as a result of the ligand functional groups. Work further exploring the generality of these trends are ongoing in our group.

The ability to maintain consistent solid-state packing across an isostructural series of porous coordination cages is somewhat unusual as control over cage packing is often dominated by interactions between incorporated functional groups. This has been demonstrated for a number of extensively studied coordination cages including isophthalate and carbazole dicarboxylate-linked paddlewheel systems as well as Cp-capped Zr cages.²⁶ Significant changes to solid-state packing upon functional group variation can influence the solubility for these systems and limit rational approaches to enhancing their solubility. Thus, calixarene-capped cages offer a somewhat unique opportunity to vary material solubility simply through

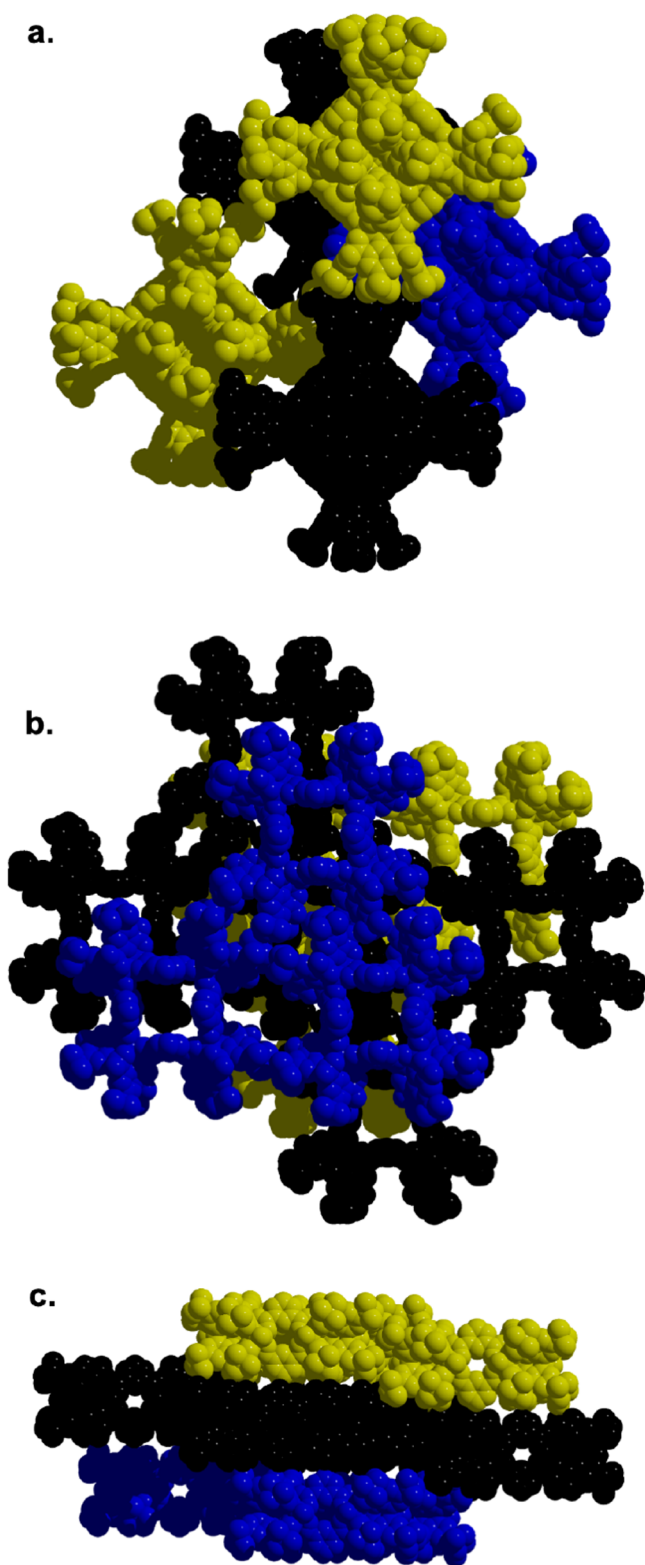


Figure 4. Solid-state packing of octahedral (a) and truncated octahedral (b, c) cages. In both structures, cage–cage interactions are governed by the *tert*-butyl groups on the cluster rather than functional groups on the dicarboxylate ligands in a specific cage.

functional group incorporation while maintaining the same solid-state packing and having a minimal effect on surface area.

As compared to carbazole dicarboxylate- or isophthalic acid-based cages, calixarene-capped cages do display a moderate

level of solubility in polar solvents, likely a result of their charged nature. The parent cage structures, M-(btc), M-(p-bdc), and M-(*m*-bdc) (M = Co²⁺, Ni²⁺), are moderately soluble in DMF, chloroform, and methylene chloride. The truncated structures are additionally soluble in acetone and THF. With eight newly synthesized materials in hand, we sought to survey the solubility of these cages as a function of structure type and functional group. It is notable that the solubility of as-synthesized cages was generally low and was somewhat irreproducible from batch to batch. Solvent exchange and activation of cages prior to solubility screening gave straightforward results, and cages typically displayed higher solubilities after such treatment. The results of these tests are listed in Table 1. The solubility of octahedral cages increases with the addition of functional groups on the bridging ligands of the cage. For instance, while the parent nickel cage is soluble in DMF, chloroform, methylene chloride, and acetone, the same octahedral cage bridged by *dobdc*^{4−} ligands exhibits solubility in at least three additional solvents including tetrahydrofuran, benzene, and toluene. Comparatively, truncated octahedral cages exhibit slightly different solubility characteristics than octahedral cages when functionalized. This is due to the location of the functional group residing closer to the outermost periphery of the cage, lending more influence toward solubility in comparison to terephthalate-based cages. The parent cobalt and nickel *m*-bdc cages have less solubility when compared to the hydrocarbon and alkoxy-functionalized analogues reported here. The addition of a simple methyl group on the isophthalate ligand leads to a highly soluble cage that can also be dissolved in benzene, toluene, and ethyl acetate. As seen in Table 1, increasing the size of the appended functional group generally increases the solubility of the cage. Conversely, Ni-(5-Sulfo) and Co-(5-Sulfo) are insoluble in all nonpolar and most polar solvents we employed with the exception of DMF, in which the cages remained highly soluble. This is likely a result of the higher charge of this cage (12−) as compared to cages based on ligands with neutral functional groups (4−).

The solubility of coordination cages is not only important for practical applications, where it can be leveraged for material synthesis, purification, characterization, and utilization, it is an important consideration in achieving high surface areas. In most extended network solids, samples are thoroughly washed with a high boiling synthesis solvent, typically an amide such as DMF or DMA. After this process, they are exchanged with a more volatile solvent to facilitate activation at more modest temperatures. This procedure is particularly important for MOFs with metal-bound solvent molecules as these are much more difficult to remove than pore-bound solvent. Because of the saturated coordination of the metal centers in each tetranuclear cluster of these compounds, there are no exposed metal sites for the coordination of solvent molecules. Given their solubility in a range of solvents, particularly DMF, we were able to forego exchanges with highly polar solvents. We were somewhat limited, however, in which volatile solvents could be used. Ultimately, room temperature washes with EtOH were sufficient for removing DMF and unreacted metal, ligand, or calixarene cap from the materials reported here. Fully exchanged samples, as determined by the absence of a C=O carbonyl stretch in the IR spectra of exchanged samples (Figures S6–S24), were dried under dynamic vacuum at room temperature before being transferred to gas adsorption tubes for screening of optimal activation temperatures. For these, we

utilized flowing N₂ rather than dynamic vacuum as it more similarly represents the experimental parameters used in TGA experiments (Figures S25–S32).

As is often the case for MOFs, when comparing the optimal activation temperatures of these materials with their respective TGA measurements, there is no clear correlation between the two. The TGA measurements are similar across all materials tested where there is a slight decrease in weight percent due to loss of solvent below 100 °C followed by a long plateau in weight percent and apparent decomposition at ~400 °C. Regardless, the plateau between solvent loss and decomposition shows no notable loss of weight that would give insight into activation temperature. As a result, sample activation screens were necessary to determine the optimum activation temperature of each material. Temperature screens were performed by activating samples at 25 °C intervals under dynamic nitrogen flow from room temperature until gas uptake decreased drastically (loss of ~0.5–1.0 mmol/g). We generally found that optimal activation, as judged by N₂ or CO₂ adsorption at 77 or 195 K, respectively, was achieved upon heating samples to approximately 200–250 °C (Figures S33–S45). Based on the evidence from the TGA measurements, all solvent was evacuated from the system by 200 °C, which suggests any change in uptake of N₂ or CO₂ from 200 to 400 °C is due to an alteration in the crystal packing of the system and/or thermal decomposition.

Table 2. Surface Areas of Cages

cage	BET SA (m ² /g) (N ₂)	Lang SA (m ² /g) (N ₂)	BET SA (m ² /g) (CO ₂)	Lang SA (m ² /g) (CO ₂)
Ni-(btc)	230 ²⁹			
Ni-(<i>p</i> -bdc)	523 ⁴⁵			
Co-(<i>p</i> -bdc)	423 ⁴⁵			
Ni-(<i>m</i> -bdc)	803 ⁴⁶			
Co-(5-Sulfo)	238	476	262	406
Ni-(2-Methyl)	437	607	291	516
Ni-(5-Methyl)	442	649	291	536
Ni-(2-Br)	410	551	286	479
Ni-(5-Br)	596	749	391	552
Ni-(dobdc)	592	849	379	690
Ni-(5-OProp)	403	808	314	460
Co-(5-OHept)	22	25	252	507

A clear advantage of calixarene-capped cages is their solid-state packing is largely governed by the nature of the capping ligand rather than the bridging di- or tricarboxylate ligands that connect their tetranuclear clusters. As a result, while it is expected that dramatic ligand functionalization will have a negative effect on material surface area (Figures S92–S107), dramatic tuning of solubility can be achieved. Surface areas of previously reported cages generally support this hypothesis as the gas adsorption characteristics of Ni-(*p*-bdc), Ni-(btc), and Ni-(5-Sulfo) have been measured by Wang and co-workers and show N₂ uptakes (at 77 K and 1.0 bar) of 8.01, 8.96, and 5.13 mmol/g, respectively, and CO₂ (at 195 K and 1.0 bar) uptakes of 7.27, 7.70, and 5.69 mmol/g, respectively. Upon comparison

of these materials to the functionalized analogues reported here, there is a slight decrease in uptake upon functional group incorporation. The greatest decrease in gas adsorption in a terephthalic acid cage is seen with Ni-(2-Br), which decreases to 5.75 and 5.18 mmol/g for N₂ and CO₂, respectively, as compared to 8.01 and 7.27 mmol/g. The decrease in gravimetric uptake and surface area is expected given the significantly increased molar mass of the 2-Br-bdc²⁻ as compared to *p*-bdc²⁻. The truncated cage with the greatest decrease as compared to its unfunctionalized analogue is Co-(5-Heptoxy), which displays saturation uptakes of just of 0.33 and 5.10 mmol/g for N₂ and CO₂, respectively. The trends in gas uptake and surface area correlate with the positioning of the functional group for each cage type. With the addition of a functional group to an octahedral cage, the organic moiety sits at the edge of the pore window. This reduces the availability for gas to access the interior surface of the cage while the extra-cage surface area is unchanged. On the other hand, upon examination of truncated cages, the functional group must be oriented away from the internal void of the cage; it does not take up any space in the internal pore, although it can restrict access to the pore which can inhibit uptake of gas. With the addition of increasing sterically hindering groups this reduction in pore window diameter only becomes more drastic, which can explain the reduction in N₂ adsorption in Ni-(5-Prop) and Co-(5-Hept). Co-(5-OHept), for example, is minimally porous to N₂ while it has a CO₂ accessible surface area on par with the other cages.

The tunable solubility of these cages can be leveraged for mechanical shaping and/or monolith formation. We have previously focused on the densification of cage materials via solvent processing. However, because of the increased recent interest in mechanical shaping of MOFs, application of these methods into cage systems is worth exploring. While methods for manual shaping of MOFs, including pressing,⁵³ spray drying,⁵⁴ and granulation,⁵⁵ have been reported, methods applied to porous cages have been limited. We initiated a proof-of-concept study to show how functionalized calixarene-capped cages can be used to create mechanically shaped porous materials while still retaining the gravimetric uptake and surface area of unaltered counterparts.

Ni-(2-Methyl), Ni-(5-Methyl), and Ni-(5-OProp), are highly soluble in benzene which allows them to be isolated as activated materials upon sublimation of solvent from frozen samples. In this approach, the three cages largely retained their shape immediately following this benzene freeze-drying (Bz FD) procedure (Figure S140). Nitrogen adsorption isotherms collected at 77 K confirmed that the cages retained gravimetric surface area as compared to their counterparts activated under more typical conditions with Ni-(2-Methyl)Bz FD, Ni-(5-Methyl)Bz FD, and Ni-(5-OProp)Bz FD exhibiting BET surface areas of 418, 425, and 421 m²/g, respectively (Figures S108–S111). This supports the idea that manipulation of these cages in the solid state has minimal influence over their ability to adsorb gas making these materials good candidates for mechanical shaping in the future. To further investigate volume tuning of these materials, we focused on Ni-(2-Methyl) as it maintains a robust structure upon freeze-drying, and it can potentially be used to afford product phases with tunable densities. Here, simply tuning the concentration of starting solutions can be leveraged to adjust the density of shaped product phases. Three solutions of constant volume and varying cage concentrations were prepared, frozen, and the

solvent was sublimed to afford porous product where the density and mechanical stability are highly tunable (Figure S141).

CONCLUSIONS

We have described a series of calixarene-capped porous coordination cages that can be synthesized in a modular fashion using a broad range of functionalized terephthalic and isophthalic bridging ligands. The terephthalic acid-based cages presented in this work generally crystallize in the $R\bar{3}$ space group regardless of the functional group present on the bridging ligand as cage–cage interactions are instead governed by the nature of the calixarene cap. Similarly, the packing of isophthalic acid-based cages in the solid state is largely based on cap–cap interactions rather than the functional groups on the 5-position of the isophthalic acid ligands they are based on. The solubility of both types of cages increases significantly with the addition of functional groups to their bridging ligands, exhibiting subtle decreases in their surface areas. It is expected that utilization of extended linear and bent linkers with appropriate functional groups will lead to a large class of highly porous cages that importantly still exhibit the hallmark solubility of porous coordination cages. In addition, the improved solubility of these materials compared to other cage complexes offers potential benefits for a variety of applications, most notably mechanical shaping for future applications in gas adsorption that have virtually been exclusive to MOFs. These observations motivate our ongoing interest in expanding the chemistry of molecular metal–organic materials to complement studies of MOFs.

ASSOCIATED CONTENT

Supporting Information

The Supporting Information is available free of charge at <https://pubs.acs.org/doi/10.1021/acs.inorgchem.0c03554>.

Synthetic details, crystal structure details, and gas adsorption plots (PDF)

Accession Codes

CCDC 2016862–2016867 contain the supplementary crystallographic data for this paper. These data can be obtained free of charge via www.ccdc.cam.ac.uk/data_request/cif, or by emailing data_request@ccdc.cam.ac.uk, or by contacting The Cambridge Crystallographic Data Centre, 12 Union Road, Cambridge CB2 1EZ, UK; fax: +44 1223 336033.

AUTHOR INFORMATION

Corresponding Author

Eric D. Bloch – Department of Chemistry and Biochemistry, University of Delaware, Newark, Delaware 19716, United States; orcid.org/0000-0003-4507-6247; Email: edb@udel.edu

Authors

Michael R. Dworzak – Department of Chemistry and Biochemistry, University of Delaware, Newark, Delaware 19716, United States

Meaghan M. Deegan – Department of Chemistry and Biochemistry, University of Delaware, Newark, Delaware 19716, United States

Glenn P. A. Yap – Department of Chemistry and Biochemistry, University of Delaware, Newark, Delaware 19716, United States

Complete contact information is available at:

<https://pubs.acs.org/doi/10.1021/acs.inorgchem.0c03554>

Funding

This material is based upon work supported by the U.S. Department of Energy's Office of Energy Efficiency and Renewable Energy under the Hydrogen and Fuel Cell Technologies and Vehicle Technologies Offices under Award DE-EE0008813.

Notes

The authors declare no competing financial interest.

REFERENCES

- (1) Lorzing, G. R.; Trump, B. A.; Brown, C. M.; Bloch, E. D. Selective Gas Adsorption in Highly Porous Chromium(II)-Based Metal–Organic Polyhedra. *Chem. Mater.* **2017**, *29*, 8583–8587.
- (2) Kewley, A.; Stephenson, A.; Chen, L.; Briggs, M. E.; Hasell, T.; Cooper, A. I. Porous Organic Cages for Gas Chromatography Separations. *Chem. Mater.* **2015**, *27*, 3207–3210.
- (3) Duriska, M. B.; Neville, S. M.; Lu, J.; Iremonger, S. S.; Boas, J. F.; Kepert, C. J.; Batten, S. R. Systematic Metal Variation and Solvent and Hydrogen–Gas Storage in Supramolecular Nanoballs. *Angew. Chem., Int. Ed.* **2009**, *48*, 8919–8922.
- (4) Evans, J. D.; Huang, D. M.; Hill, M. R.; Sumbly, C. J.; Sholl, D. S.; Thornton, A. W.; Doonan, C. J. Molecular Design of Amorphous Porous Organic Cages for Enhanced Gas Storage. *J. Phys. Chem. C* **2015**, *119*, 7746–7754.
- (5) Murase, T.; Nishijima, K.; Fujita, M. Cage-Catalyzed Knoevenagel Condensation under Neutral Conditions in Water. *J. Am. Chem. Soc.* **2012**, *134*, 162–164.
- (6) Ng, C. K.; Toh, R. W.; Lin, T. T.; Luo, H.-K.; Hor, T. S. A.; Wu, J. Metal–salen Molecular Cages as Efficient and Recyclable Heterogeneous Catalysts for Cycloaddition of CO₂ with Epoxides Under Ambient Conditions. *Chem. Sci.* **2019**, *10*, 1549–1554.
- (7) Bilbeisi, R. A.; Clegg, J. K.; Elgrishi, N.; de Hatten, X.; Devillard, M.; Breiner, B.; Mal, P.; Nitschke, J. R. Subcomponent Self-Assembly and Guest-Binding Properties of Face-Capped Fe₄L₄⁸⁺ Capsules. *J. Am. Chem. Soc.* **2012**, *134*, 5110–5119.
- (8) Percastegui, E. G.; Mosquera, J.; Ronson, T. K.; Plajer, A. J.; Kieffer, M.; Nitschke, J. R. Waterproof Architectures Through Subcomponent Self-Assembly. *Chem. Sci.* **2019**, *10*, 2006–2018.
- (9) Taylor, L. L. K.; Riddell, I. A.; Smulders, M. M. J. Self-Assembly of Functional Discrete Three-Dimensional Architectures in Water. *Angew. Chem., Int. Ed.* **2019**, *58*, 1280–1307.
- (10) Jones, J. T. A.; Hasell, T.; Wu, X.; Bacsa, J.; Jelfs, K. E.; Schmidtman, M.; Chong, S. Y.; Adams, D. J.; Trewin, A.; Schifman, F.; Cora, F.; Slater, B.; Steiner, A.; Day, G. M.; Cooper, A. I. Modular and Predictable Assembly of Porous Organic Molecular Crystals. *Nature* **2011**, *474*, 367–371.
- (11) Chen, B.; Holstein, J. J.; Horiuchi, S.; Hiller, W. G.; Clever, G. H. Pd(II) Coordination Sphere Engineering: Pyridine Cages, Quinoline Bowls, and Heteroleptic Pill Binding One or Two Fullerenes. *J. Am. Chem. Soc.* **2019**, *141*, 8907–8913.
- (12) Liu, G.; Di Yuan, Y.; Wang, J.; Cheng, Y.; Peh, S. B.; Wang, Y.; Qian, Y.; Dong, J.; Yuan, D.; Zhao, D. Process-Tracing Study on the Postassembly Modification of Highly Stable Zirconium Metal–Organic Cages. *J. Am. Chem. Soc.* **2018**, *140*, 6231–6234.
- (13) Naseer, M. M.; Wang, D.-X.; Zhao, L.; Wang, M.-X. Construction and Multiple Exterior Surface Functionalization of Giant Molecular Cages. *Eur. J. Org. Chem.* **2014**, *2014*, 7895–7905.
- (14) Hasell, T.; Schmidtman, M.; Stone, C. A.; Smith, M. W.; Cooper, A. I. Reversible Water Uptake by a Stable Imine-Based Porous Organic Cage. *Chem. Commun.* **2012**, *48*, 4689–4691.
- (15) Liu, M.; Little, M. A.; Jelfs, K. E.; Jones, J. T. A.; Schmidtman, M.; Chong, S. Y.; Hasell, T.; Cooper, A. I. Acid- and Base-Stable Porous Organic Cages: Shape Persistence and pH Stability via Post-synthetic “Tying” of a Flexible Amine Cage. *J. Am. Chem. Soc.* **2014**, *136*, 7583–7586.

- (16) McTernan, C. T.; Ronson, T. K.; Nitschke, J. R. Post-assembly Modification of Phosphine Cage Controls Host-Guest Behavior. *J. Am. Chem. Soc.* **2019**, *141*, 6837–6842.
- (17) Roberts, D. A.; Pilgrim, D. S.; Sirvinskaite, G.; Ronson, T. K.; Nitschke, J. R. Covalent Post-Assembly Modification Triggers Multiple Structural Transformations of Tetrazine-Edged Fe₄L₆ Tetrahedron. *J. Am. Chem. Soc.* **2018**, *140*, 9616–9623.
- (18) Li, Y.; Wang, H.; Wang, C.; Xu, J.; Ma, S.; Ou, J.; Zhang, J.; Li, G.; Wei, Y.; Ye, M. Atomically Precise Structure Determination of Porous Organic Cage from Ab Initio PXRD Structure Analysis: Its Molecular Click Postfunctionalization and CO₂ Capture Application. *ACS Appl. Mater. Interfaces* **2020**, *12*, 17815–17823.
- (19) Konopka, M.; Cecot, P.; Ulrich, S.; Stefankiewicz, A. R. Tuning the Solubility of Self-Assembled Fluorescent Aromatic Cages Using Functionalized Amino Acid Building Blocks. *Front. Chem.* **2019**, *7*, 503.
- (20) Jin, Y.; Voss, B. A.; Jin, A.; Long, H.; Noble, R. D.; Zhang, W. Highly CO₂-Selective Organic Molecular Cages: What Determines the CO₂ Selectivity. *J. Am. Chem. Soc.* **2011**, *133*, 6650–6658.
- (21) Taggart, G. A.; Antonio, A. M.; Lorz, G. R.; Yap, G. P. A.; Bloch, E. D. Tuning the Porosity, Solubility, and Gas-Storage Properties of Cuboctahedral Coordination Cage via Amide or Ester Functionalization. *ACS Appl. Mater. Interfaces* **2020**, *12*, 24913–24919.
- (22) Barreda, O.; Bannwart, G.; Yap, G. P. A.; Bloch, E. D. Ligand-Based Phase Control in Porous Molecular Assemblies. *ACS Appl. Mater. Interfaces* **2018**, *10*, 11420–11424.
- (23) Dai, F. R.; Qiao, Y.; Wang, Z. Designing Structurally Tunable and Functionally Versatile Synthetic Supercontainers. *Inorg. Chem. Front.* **2016**, *3*, 243–249.
- (24) Carne-Sanchez, A.; Albalad, J.; Grancha, T.; Imaz, I.; Juanhuix, J.; Larpent, P.; Furukawa, S.; MasPOCH, D. Postsynthetic Covalent and Coordination Functionalization of Rhodium(II)-Based Metal-Organic Polyhedra. *J. Am. Chem. Soc.* **2019**, *141*, 4094–4102.
- (25) Gosselin, A. J.; Rowland, C. A.; Balto, K. P.; Yap, G. P. A.; Bloch, E. D. Design and Synthesis of Porous Nickel(II) and Cobalt(II) Cages. *Inorg. Chem.* **2018**, *57*, 11847–11850.
- (26) Gosselin, A. J.; Rowland, C. A.; Bloch, E. D. Permanently Microporous Metal-Organic Polyhedra. *Chem. Rev.* **2020**, *120*, 8987–9014.
- (27) Gosselin, A. J.; Decker, G. E.; McNichols, B. W.; Baumann, J. E.; Yap, G. P. A.; Sellinger, A.; Bloch, E. D. Ligand-Based Phase Control in Porous Zirconium Coordination Cages. *Chem. Mater.* **2020**, *32*, 5872–5878.
- (28) Liu, M.; Liao, W. Bridging Calixarene-Based {Co₄} Units into a Square or Belt with Aromatic Dicarboxylic Acids. *CrystEngComm* **2012**, *14*, 5727–5729.
- (29) Dai, F. R.; Wang, Z. Modular Assembly of Metal-Organic Supercontainers Incorporating Sulfonylcalixarenes. *J. Am. Chem. Soc.* **2012**, *134*, 8002–8005.
- (30) Liu, M.; Liao, W.; Hu, C.; Du, S.; Zhang, H. Calixarene-Based Nanoscale Coordination Cages. *Angew. Chem., Int. Ed.* **2012**, *51*, 1585–1588.
- (31) Du, S.; Hu, C.; Xiao, J.-C.; Tan, H.; Liao, W. A Giant Coordination Cage Based on Sulfonylcalix[4]arene. *Chem. Commun.* **2012**, *48*, 9177–9179.
- (32) Liu, M.; Du, S.; Liao, W. A Metal-Organic Coordination Nanotube Based on Co₄-TC4A Subunits and V-Shaped Aromatic Dicarboxylic Acids. *J. Mol. Struct.* **2013**, *1049*, 310–314.
- (33) Wang, S.; Gao, X.; Hang, X.; Zhu, X.; Han, H.; Liao, W.; Chen, W. Ultrafine Pt Nanoclusters Confined in a Calixarene-Based {Ni₂₄} Coordination Cage for High-Efficient Hydrogen Evolution Reaction. *J. Am. Chem. Soc.* **2016**, *138*, 16236–16239.
- (34) Bhuvaneshwari, N.; Dai, F. R.; Chen, Z. N. Sensitive and Specific Guest Recognition through Pyridinium-Modification in Spindle-Like Coordination Containers. *Chem. - Eur. J.* **2018**, *24*, 6580.
- (35) Guérineau, V.; Rollet, M.; Viel, S.; Lepoittevin, B.; Costa, L.; Saint-Aguet, P.; Laurent, R.; Roger, P.; Gimes, D.; Martini, C.; Huc, V. The Synthesis and Characterization of Giant Calixarenes. *Nat. Commun.* **2019**, *10*, 113.
- (36) Simaan, S.; Biali, S. E. Synthesis of p-tert-Butylcalix[4]arene Derivatives with trans-Alkyl Substituents on Opposite Methylene Bridges. *J. Org. Chem.* **2003**, *68*, 3634–3639.
- (37) Kumagai, H.; Hasegawa, M.; Miyanari, S.; Sugawa, Y.; Sato, Y.; Hori, T.; Ueda, S.; Kamiyama, H.; Miyano, S. Facile Synthesis of p-tert-butylthiacalix[4]arene by the Reaction of p-tert-butylphenol with Elemental Sulfur in the Presence of a Base. *Tetrahedron Lett.* **1997**, *38*, 3971–3972.
- (38) Fang, Y.; Li, J. L.; Togo, T.; Jin, F. Y.; Xiao, Z. F.; Liu, L. J.; Drake, H.; Lian, X. Z.; Zhou, H. C. Ultra-Small Face-Centered-Cubic Ru Nanoparticles Confined within a Porous Coordination Cage for Dehydrogenation. *Chem.* **2018**, *4*, 555–563.
- (39) Iki, N.; Kumagai, H.; Morohashi, N.; Ejima, K.; Hasegawa, M.; Miyanari, S.; Miyano, S. Selective Oxidation of Thiacalix[4]arenes to the Sulfinyl- and Sulfonylcalix[4]arenes and Their Coordination Ability to Metal Ions. *Tetrahedron Lett.* **1998**, *39*, 7559–7562.
- (40) Deegan, M. M.; Ahmed, T. S.; Yap, G. P.; Bloch, E. D. Structure and Redox Tuning of Gas Adsorption Properties in Calixarene-Supported Fe(II)-Based Porous Cages. *Chem. Sci.* **2020**, *11*, 5273–5279.
- (41) Gutsche, C. D.; Dhawan, B.; No, K. H.; Muthukrishnan, R. Calixarenes. 4. The Synthesis, Characterization, and Properties of the Calixarenes from p-tert-butylphenol. *J. Am. Chem. Soc.* **1981**, *103*, 3782–3792.
- (42) Du, S.; Yu, T.-Q.; Liao, W.; Hu, C. Structure Modeling, Synthesis and X-ray Diffraction Determination of an Extra-Large Calixarene-Based Coordination Cage and its Application in Drug Delivery. *Dalton Trans.* **2015**, *44*, 14394–14402.
- (43) Gueneau, E. D.; Fromm, K. M.; Goesmann, H. Synthesis and Structural Analysis of the Polymetallated Alkali Calixarenes [M₄(p-tert-butylcalix[4]arene-4H)(thf)_x]₂•n THF (M = Li, K; n = 6 or 1; x = 4 or 5) and [Li₂(p-tert-butylcalix[4]arene-2H)(H₂O)(μ-H₂O)(thf)•3 THF. *Chem. - Eur. J.* **2003**, *9*, 509–514.
- (44) Zhu, X.; Wang, S.; Han, H.; Liao, W. Organoamine-induced Isomerism of Calixarene-Based Complexes: from 1D to 2D. *RSC Adv.* **2018**, *8*, 39208–39213.
- (45) Dai, F. R.; Sambasivam, U.; Hammerstrom, A. J.; Wang, Z. Synthetic Supercontainers Exhibit Distinct Solution versus Solid State Guest-Binding Behavior. *J. Am. Chem. Soc.* **2014**, *136*, 7480–7491.
- (46) Dai, F. R.; Becht, D. C.; Wang, Z. Modulating Guest Binding in Sulfonylcalixarene-based Metal-Organic Supercontainers. *Chem. Commun.* **2014**, *50*, 5385–5387.
- (47) Huang, X.; Yang, L.; Bergquist, J.; Strømme, M.; Gogoll, A.; Sjödin, M. Synthesis and Redox Properties of Thiophene Terephthalate Building Blocks for Low-Potential Conducting Redox Polymers. *J. Phys. Chem. C* **2015**, *119*, 27247–27254.
- (48) Antonio, A. M.; Korman, K. J.; Yap, G. P. A.; Bloch, E. D. Porous Metal-Organic Alloys Based on Soluble Coordination Cages. *Chem. Sci.* **2020**, *11*, 12540.
- (49) Apex3; Bruker AXS Inc.: Madison, WI, 2015.
- (50) Sheldrick, G. M. SHELXT-Integrated Space-Group and Crystal Structure Determination. *Acta Crystallogr.* **2015**, *A71*, 3–8.
- (51) Dolomanov, O. V.; Bourhis, L. J.; Gildea, R. J.; Howard, J. A. K.; Puschmann, H. OLEX2: A Complete Structure Solution, Refinement and Analysis Program. *J. Appl. Crystallogr.* **2009**, *42*, 339–341.
- (52) Li, C.-P.; Chen, J.; Yu, Q.; Du, M. Structural Modulation and Properties of Silver(I) Coordination Frameworks with Benzenedicarboxyl Tectons and trans-1-(2-Pyridyl)-2-(4-pyridyl)ethylene Spacer. *Cryst. Growth Des.* **2010**, *10*, 1623–1632.
- (53) Peng, Y.; Krungleviciute, V.; Eryazici, I.; Hupp, J. T.; Farha, O. K.; Yildirim, T. Methane Storage in Metal-Organic Frameworks: Current Records, Surprise Findings, and Challenges. *J. Am. Chem. Soc.* **2013**, *135*, 11887–11894.
- (54) Carné-Sánchez, A.; Imaz, I.; Cano-Sarabia, M.; MasPOCH, D. A Spray-Drying Strategy for Synthesis of Nanoscale Metal-Organic

Frameworks and their Assembly into Hollow Substructures. *Nat. Chem.* **2013**, *5*, 203–211.

(55) Spjelkavik, A. I.; Aarti; Divekar, S.; Didriksen, T.; Blom, R. Forming MOFs into Spheres by use of Molecular Gastronomy Methods. *Chem.—Eur. J.* **2014**, *20*, 8973–8978.